Numerical study of the two-dimensional Hubbard model

S. R. White, D. J. Scalapino, and R. L. Sugar
Department of Physics, University of California, Santa Barbara, Santa Barbara, California 93106

E. Y. Loh and J. E. Gubernatis
Theoretical Division, Los Alamos National Laboratory, Los Alamos, New Mexico 87545

R. T. Scalettar
Department of Physics, University of Illinois, Urbana-Champaign, Urbana, Illinois 61801
(Received 19 December 1988)

We report on a numerical study of the two-dimensional Hubbard model and describe two new algorithms for the simulation of many-electron systems. These algorithms allow one to carry out simulations within the grand canonical ensemble at significantly lower temperatures than had previously been obtained and to calculate ground-state properties with fixed numbers of electrons. We present results for the two-dimensional Hubbard model with half- and quarter-filled bands. Our results support the existence of long-range antiferromagnetic order in the ground state at half-filling and its absence at quarter-filling. Results for the magnetic susceptibility and the momentum occupation along with an upper bound to the spin-wave spectrum are given. We find evidence for an attractive effective d-wave pairing interaction near half-filling but have not found evidence for a phase transition to a superconducting state.

I. INTRODUCTION

In this paper we report on a numerical study of the two-dimensional Hubbard model. We present and make use of two new algorithms for the simulation of many-electron systems which make use of matrix-decomposition methods to stabilize the calculation of fermion determinants and Green's functions. One of the algorithms allows simulations within the grand canonical ensemble to be performed at significantly lower temperatures than have previously been obtained. The other allows direct calculations of ground-state properties of systems with fixed numbers of electrons.[1]

A major problem in the numerical simulation of many-electron systems has been to carry out calculations at sufficiently low temperatures. The problems is essentially one of energy scales. The collective phenomena of interest, such as magnetism or superconductivity, have characteristic energy scales 10 to 1,000 times smaller than the bandwidth or Coulomb interaction strength. The difficulty in achieving temperatures low enough to probe these energy scales is the need to evaluate repeatedly the determinant or inverse of a fermion matrix that becomes increasingly ill-conditioned as the temperature is lowered. Indeed, the fermion matrix has eigenvalues which grow exponentially with the inverse temperature, β. These eigenvalues are associated with low-lying negative energy states which are rarely unfilled. On the other hand, for the grand canonical ensemble the fermion matrix has eigenvalues quite close to one, associated with states having large positive energy, which are rarely occupied. Of course, such a wide range of eigenvalues creates considerable difficulty in the numerical evaluation of the determinant or inverse of the fermion matrix.

Recently, algorithms have been developed which allow simulations to be carried out within the grand canonical ensemble at low temperatures.[2] In these approaches the original fermion matrix, which has dimension equal to the spatial volume of the lattice, V, is replaced by a larger, but generally better conditioned matrix. Since the computer time needed to calculate the determinant or inverse of a fermion matrix grows rapidly with its dimension, these algorithms tend to be slow at low temperatures. In this paper we describe a new algorithm for the grand canonical ensemble which allows us to work directly with the V-dimensional fermion matrix. Through the use of matrix-decomposition methods, this algorithm deals directly with the causes of the ill-conditioning, and remains stable at arbitrarily low temperatures. For temperatures 10^{-2} to 10^{-3} times the bandwidth, it is significantly faster than the algorithms of Ref. 2, and it has allowed us to perform simulations at significantly lower temperatures than have been previously reported. We also present a Monte Carlo algorithm for calculating ground-state properties which uses the same stabilization methods. This algorithm uses a fermion matrix of dimension equal to the number of electrons being simulated, and may have a significant advantage for low-density band fillings. However, for higher densities within the parameter regions we have studied, it is faster to obtain zero-temperature results using the grand-canonical ensemble at low temperatures, than it is to use the ground-state algorithm.

Our development of these algorithms was stimulated by the work of Sugiyama and Koonin[3] and of Sorella *et al.*,[4] who recently reported on simulations of ground-state properties of the two-dimensional Hubbard model. Their algorithm uses Langevin dynamics to project out

the ground state from a trial state with a fixed number of electrons. A key elements in their algorithm is the use of an orthogonalization procedure to separate the diverse energy scales that are present in the fermion matrix, and thereby stabilize their calculation. We use a similar orthogonalization procedure to stabilize the calculation of the fermion matrices. Our zero-temperature approach differs from that of Sorella *et al.* in that it makes use of an exact updating, Monte Carlo method which avoids the finite step-size errors inherent in the Langevin equations. The grand-canonical algorithm furthers differs from the approach of Sorella *et al.* in that it allows calculations at finite temperature.

In Sec. II we introduce our algorithms by applying them to the two-dimensional Hubbard model. In Sec. III we give results for energies, momentum occupation, and various equal-time correlation functions for both half-filling, $\langle n \rangle = 1.0$, and quarter-filling, $\langle n \rangle = 0.5$. Low-temperature limits of the grand canonical ensemble are compared with zero-temperature results for fixed numbers of electrons. For the half-filled band our simulations are performed on large enough lattices to allow an extrapolation to the infinite system. We find evidence for long-range antiferromagnetic order in the ground state, in agreement with previous work of Hirsch and Tang.[5] Near half-filling we find evidence for an attractive effective d-wave pairing interaction, but not for a phase transition to a superconduction state. The problem associated with the sign of the fermion determinants for the non-half-filled band is also discussed. With the low-temperature stability of the new algorithm, this is the only major problem remaining in the simulation of many-electron systems.

II. THE ALGORITHMS

A. The grand-canonical ensemble

The basic approach for simulating the grand-canonical ensemble was formulated some time ago,[6] but we outline it here in order to make this paper reasonably self-contained. The expectation value of a physical observable, O, is given by

$$\langle O \rangle = \frac{\mathrm{Tr}(Oe^{-\beta H})}{\mathrm{Tr}(e^{-\beta H})} , \tag{1}$$

where β is the inverse temperature, and H is the Hamiltonian. For the Hubbard model

$$H = -t \sum_{\langle ij \rangle, \sigma} (c_{i\sigma}^{\dagger} c_{j\sigma} + c_{j\sigma}^{\dagger} c_{i\sigma}) + U \sum_i (n_{i+} - \tfrac{1}{2})(n_{i-} - \tfrac{1}{2}) - \mu \sum_i (n_{i+} + n_{i-}) . \tag{2}$$

Here $c_{i\sigma}^{\dagger}$ and $c_{i\sigma}$ are the creation and annihilation operators for electrons with a z component of spin σ at lattice site i, and $n_{i\sigma} = c_{i\sigma}^{\dagger} c_{i\sigma}$. The sum $\langle ij \rangle$ is over all pairs of nearest neighbor lattice sites. t is the hopping parameter, μ the chemical potential, and U the Coulomb coupling constant, which we take to be positive.

In order to perform a numerical simulation, we must first carry out the traces over the fermion degrees of freedom. To this end we introduce a small imaginary-time step, $\Delta\tau$ by writing $\beta = \Delta\tau L$. The partition function can then be written in the form

$$Z = \mathrm{Tr}(e^{-\Delta\tau L H}) \simeq \mathrm{Tr}(e^{-\Delta\tau V} e^{-\Delta\tau K})^L , \tag{3}$$

with

$$K = -t \sum_{\langle ij \rangle, \sigma} (c_{i\sigma}^{\dagger} c_{j\sigma} + c_{j\sigma}^{\dagger} c_{i\sigma}) - \mu \sum_i (n_{i+} + n_{i-}) = \sum_{\langle ij \rangle, \sigma} c_{i\sigma}^{\dagger} k_{ij} c_{j\sigma} \tag{4}$$

and

$$V = U \sum_i (n_{i+} - \tfrac{1}{2})(n_{i-} - \tfrac{1}{2}) . \tag{5}$$

The Trotter formula[7] used in Eq. (3) introduces errors in measured quantities of order $\Delta\tau^2$.[8] This is the only source of systematic error in the calculations other than that caused by roundoff errors. The interaction terms, $\exp(-\Delta\tau V)$, can be made quadratic in the fermion creation and annihilation operators by introducing Hirsch's discrete Hubbard-Stratonovich transformation[9]

$$e^{-\Delta\tau U(n_{i+} - \frac{1}{2})(n_{i-} - \frac{1}{2})} = e^{-\Delta\tau U/4} \frac{1}{2} \sum_{s_{i,l} = \pm 1} e^{-\Delta\tau s_{i,l} \lambda (n_{i+} - n_{i-})} \tag{6}$$

at each lattice point, i, and each imaginary-time slice, l. λ is defined by the relation $\cosh(\Delta\tau\lambda) = \exp(\Delta\tau U/2)$. The transformation reduces the quartic self-interaction of the electrons to a quadratic interaction with the Hubbard-Stratonovich spin field, $s_{i,l}$. As a result, the trace over electron degrees of freedom can be performed yielding[6]

$$Z = \sum_{s_{i,l} = \pm 1} \det M^{+} \det M^{-} , \tag{7}$$

with

$$M^{\sigma} = I + B_L^{\sigma} B_{L-1}^{\sigma}, \ldots, B_1^{\sigma} \tag{8}$$

and

$$B_l^{\pm} = e^{\mp \Delta\tau \lambda \nu(l)} e^{-\Delta\tau k} . \tag{9}$$

I is the $V \times V$ unit matrix and $\nu(l)_{ij} = \delta_{ij} s_{i,l}$. There is, of course, an analogous expression for the trace in the numerator of Eq. (1). The physical observable, O, ordinarily can be expressed in terms of Green's functions for the electrons propagating through the field $s_{i,l}$, that is in terms of the matrix of $1/M^{\sigma}$.[6]

Once the trace over the electron degrees of freedom has been performed, we can use standard Monte Carlo techniques to evaluate the right-hand side of Eq. (1). We wish to obtain a sequence of spin configurations, $\{s_{i,l}\}$, with a probability distribution $Z^{-1} \det M^{+} \det M^{-}$. To this end, we sweep through the lattice many times updating one spin variable at a time. Notice that the determinant of M^{σ} is unchanged by a cyclic permutation of the B_l^{σ}. So in order to update the spins on the l^{th} time slice we write

$$\det M^{\sigma} = \det(I + B_l^{\sigma}, \ldots, B_1^{\sigma} B_L^{\sigma}, \ldots, B_{l+1}^{\sigma}) = \det[I + A^{\sigma}(l)] \ . \quad (10)$$

Now in order to update the spin variable $s_{i,l}$ using any standard algorithm, such as heat bath or Metropolis, we must calculate the change in the fermion determinants when $s_{i,l} \rightarrow -s_{i,l}$. Under this change,

$$A^{\sigma}(l) \rightarrow A^{\sigma}(l)' = [I + \Delta^{\sigma}(i,l)] A^{\sigma}(l) \ , \quad (11)$$

where $\Delta^{\sigma}(i,l)$ is a matrix with only one nonzero element,

$$\Delta^{\pm}(i,l)_{jk} = \delta_{ji}\delta_{ki}(e^{\pm 2\Delta\tau\lambda s_{i,l}} - 1) \ . \quad (12)$$

The ratio of determinants after and before the spin flip is

$$R^{\sigma} = \frac{\det M^{\sigma'}}{\det M^{\sigma}} = \det[I + G^{\sigma}(l)\Delta^{\sigma}(i,l) A^{\sigma}(l)] = 1 + [1 - G^{\sigma}(l)_{ii}]\Delta^{\sigma}(i,l)_{ii} \ . \quad (13)$$

$G^{\sigma}(l)$ is the equal-time Green's function for an electron propagating through the field produced by the $s_{i,l}$.

$$G^{\sigma}(l)_{ij} = \langle T[c_{i\sigma}(l\Delta\tau) c_{j\sigma}^{\dagger}(l\Delta\tau)] \rangle = [I + A^{\sigma}(l)]_{ij}^{-1} \ . \quad (14)$$

Thus the calculation of the determinant ratios needed to carry out an individual Monte Carlo step is trivial provided one can evaluate the equal-time Green's functions.

If the equal-time Green's function $G^{\sigma}(l)$ is known, and the spin $s_{i,l}$ is flipped, then its new value, $G^{\sigma}(l)'$, can be evaluated through the relation

$$G^{\sigma}(l)' = G^{\sigma}(l) - G^{\sigma}(l)\Delta^{\sigma}(i,l) A^{\sigma}(l) G^{\sigma}(l)' = G^{\sigma}(l) - \frac{G^{\sigma}(l)\Delta^{\sigma}(i,l)[I - G^{\sigma}(l)]}{\{1 + [1 - G^{\sigma}(l)_{ii}]\Delta^{\sigma}(i,l)_{ii}\}} \ . \quad (15)$$

Since $\Delta^{\sigma}(i,l)$ has only one nonzero element, there is really no matrix multiplication in Eq. (15), and it takes V^2 operations to update the $V \times V$ matrix, $G^{\sigma}(l)$, after a spin is flipped.

After all the spins on a given time slice have been updated, we can obtain the equal-time Green's functions on the next time slice through the relations

$$G^{\sigma}(l+1) = B_{l+1}^{\sigma} G^{\sigma}(l) B_{l+1}^{\sigma -1} \ . \quad (16)$$

Since the B_l^{σ} are sparse matrices,[10] this operations takes of order V^2 numerical operations.

We have now assembled all of the ingredients necessary to carry out a simulation. Indeed, this algorithm has been used to study a wide variety of many-electron models. Since the computing time scales as V^3, its use has been restricted to one- and two-dimensional systems, and small three-dimensional ones. In past applications of the algorithm, numerical instabilities have prevented its use at low temperatures. For example, in the case of the two-dimensional Hubbard model, one is restricted to $\beta \leq 4/t$ for moderate values of U. In order to remove these instabilities, we must first understand their cause. They are not associated with the updating of the equal-time Green's function given in Eq. (15). Indeed, we have found that by staying on the same time slice one can update tens of thousands of spins without accumulating numerical errors. On the other hand, the process of advancing the equal-time Green's function to a new time slice given in Eq. (16) does introduce numerical errors, so one must periodically recompute the Green's function from scratch. In order to do so, one must compute the matrices $A^{\sigma}(l)$ to sufficient accuracy to incorporate information concerning its small eigenvalues. This becomes increasingly difficult as the temperature is lowered. For example, for the two-dimensional Hubbard model with $U=0$, the $A^{\sigma}(l)$ have eigenvalues as large as $\exp(4t\beta)$ and as small as $\exp(-4t\beta)$. Since we are interested in performing simulations for β at least as large as $20/t$, it is clear that we must separate the contributions from the large and small eigenvalues, or else the latter will be completely swamped by round-off errors.

This problem can be dealt with in a relatively straightforward manner using matrix factorization methods.[1,11] Suppose that one can multiply m of the B_l^{σ} without losing numerical accuracy. We then use the Gram-Schmidt orthogonalization procedure to write this product in the form

$$a_1^{\sigma}(l) = B_{l+m}^{\sigma} B_{l+m-1}^{\sigma}, \ldots, B_{l+1}^{\sigma} = U_1^{\sigma} D_1^{\sigma} R_1^{\sigma} \ , \quad (17)$$

where U_1^{σ} is an orthogonal matrix, D_1^{σ} a diagonal matrix, and R_1^{σ} a right triangular matrix with diagonal elements equal to one. The orthogonal matrix U_1^{σ} is necessarily well conditioned; *a priori*, R_1^{σ} need not be well conditioned, but in practice it is. Only the diagonal matrix D_1^{σ} has large variations in the size of its elements.

We next form

$$a_2^{\sigma}(l) = B_{l+2m}^{\sigma}, \ldots, B_{l+1}^{\sigma} = B_{l+2m}^{\sigma}, \ldots, B_{l+m+1}^{\sigma} U_1^{\sigma} D_1^{\sigma} R_1^{\sigma} = U_2^{\sigma} D_2^{\sigma} R_2^{\sigma} \ . \quad (18)$$

The order of operations in Eq. (18) is important. We first multiply U_1^{σ} by $B_{l+2m}^{\sigma}, \ldots, B_{l+m+1}^{\sigma}$. By assumption, m is small enough so that this matrix can be computed accurately. We then multiply it on the right by D_1^{σ}. This only rescales the columns of the matrix, and thus does no harm to the numerical stability of the next step, a *UDR* decomposition of this partial product. We then multiply the resulting triangular matrix on the right by R_1^{σ} to obtain the last line of Eq. (18). This process is repeated L/m times to obtain

$$A^{\sigma}(l) = a_{L/m}^{\sigma}(l) = U_{L/m}^{\sigma} D_{L/m}^{\sigma} R_{L/m}^{\sigma} \ . \quad (19)$$

To form $G^{\sigma}(l)^{-1}$, we must add the unit matrix to $A^{\sigma}(l)$. Care must be taken to isolate the diagonal matrix $D_{L/m}^{\sigma}$, whose elements have large variations in size. We therefore write

$$G^{\sigma}(l)^{-1} = I + A^{\sigma}(l) = U_{L/m}^{\sigma}(U_{L/m}^{\sigma -1} R_{L/m}^{\sigma -1} + D_{L/m}^{\sigma}) R_{L/m}^{\sigma} = U^{\sigma} D^{\sigma} R^{\sigma} \ . \quad (20)$$

In order to go from the second to third line of Eq. (20),

we have made a final *UDR* decomposition of the quantity in square brackets. This decomposition is numerically stable because the large and small matrix elements are again separated. The formation of $G^\sigma(l)$ from the last line of Eq. (20) is, of course, trivial. We have tested the numerical stability of our method for evaluating $G^\sigma(l)$ for values of $t\beta$ as large as 100 without encountering problems.

We conclude this discussion by examining the scaling of the simulation time with respect to lattice size and temperature. The most time consuming step in the Monte Carlo process, aside from the occasional *ab initio* calculation of the equal-time Green's functions, is their updating via Eq. (15), which requires of order V^2 operations. Therefore, the computer time required to update each of the VL spin variables is proportional to V^3L. Just as it is possible to multiply m of the B_l^σ matrices without losing numerical accuracy, it is also possible to advance the Green's functions to a new time slice, using Eq. (16), m' times without introducing unacceptable errors. Thus, one must completely recalculate the Green's functions L/m' times per lattice sweep. Since the *UDR* decomposition requires V^3 operations, the *ab initio* calculation of the Green's functions takes of order

$$V^3(L/m')(L/m)\approx V^3(L/m)^2$$

operations per sweep. We find that m and m' are roughly equal and relatively independent of temperature; requiring $t\Delta\tau m \leq 1.5$ provides a good margin of safety on a computer with 64-bit precision. As a result, if for $U=4$ we set $\Delta\tau=(8t)^{-1}$, which results in a systematic error from the Trotter approximation of a few percent, the times spent updating the spins and the time spent in the recomputation of the Green's function are comparable for β of order $20/t$. For inverse temperatures less than this, the V^3L term dominates and the computer times scales approximately linearly with β. Of course at very low temperatures it will scale like β^2, but as we will now discuss, we would then use a rather different approach.

B. Zero-temperature algorithm

It is possible to use the techniques just described to directly calculate the ground-state properties of systems with a fixed number of electrons. Let us denote by $|\Psi_0\rangle$ the ground-state wave function for N^+ spin up electrons and N^- spin down ones, and by $|\psi_0\rangle$, a trial state that has a nonzero overlap with $|\Psi_0\rangle$. Then the ground-state expectation value of a physical observable, O, can be written in the form

$$\frac{\langle\Psi_0|O|\Psi_0\rangle}{\langle\Psi_0|\Psi_0\rangle}=\lim_{\gamma,\gamma'\to\infty}\frac{\langle\psi_0|e^{-\gamma' H}Oe^{-\gamma H}|\psi_0\rangle}{\langle\psi_0|e^{-(\gamma+\gamma')H}|\psi_0\rangle}\ . \tag{21}$$

In order to evaluate the right-hand side of Eq. (21) stochastically, we write $\gamma+\gamma'=\Delta\tau L$, and use the Trotter approximation of Eq. (3) and the Hubbard-Stratonovich transformation of Eq. (6) to again integrate out the fermion degrees of freedom. We take the state $|\psi_0\rangle$ to be either one in which the electrons with z component of spin σ are localized on sites $i_1^\sigma,\ldots,i_{N^\sigma}^\sigma$ or a filled Fermi sea, the correct ground state for $U=0$. Then we can write

$$\langle\psi_0|e^{-(\gamma+\gamma')H}|\psi_0\rangle=\sum_{s_{i,l}}\det A^+\det A^-\ , \tag{22}$$

where

$$A^\sigma_{jk}=\{B^\sigma_L,\ldots,B^\sigma_1\}_{jk}\ , \tag{23}$$

and the indices j and k are restricted to run over $i_1^\sigma,\ldots,i_{N^\sigma}^\sigma$, so the A^σ are $N^\sigma\times N^\sigma$ matrices.

In order to carry out the simulation we must generate a set of spin configurations distributed as $\det A^+\det A^-$. The procedure is basically the same as for the grand-canonical ensemble. Let us imagine updating spins on time slices $nm+1$ to $(n+1)m$. Again making use of successive Gram-Schmidt orthogonalizations, we can write

$$A^\sigma=L^\sigma_L D^\sigma_L U^\sigma_L B^\sigma_{(n+1)m},\ldots,B^\sigma_{nm+1}U^\sigma_R D^\sigma_R R^\sigma_R\ , \tag{24}$$

where U^σ_R is a $V\times N^\sigma$ matrix whose columns are mutually orthogonal, and U^σ_L and $N^\sigma\times V$ matrix whose rows are mutually orthogonal. $D^\sigma_{R,L}$ are $N^\sigma\times N^\sigma$ diagonal matrices, and R^σ_R and L^σ_L are $N^\sigma\times N^\sigma$ right and left triangular matrices with unit diagonal elements. Once more, the diagonal matrices are the only ones with large variations in the size of their matrix elements. Suppose we update $s_{i,l}$, where $(n+1)m\geq l\geq nm+1$. If this spin is flipped, then $A^\sigma\to A^{\sigma'}$ with

$$\begin{aligned}A^{\sigma'}&=A^\sigma+L^\sigma_L D^\sigma_L U^\sigma_L B^\sigma_{(n+1)m},\ldots,B^\sigma_{l+1}\Delta^\sigma(i,l)B^\sigma_l,\ldots,B^\sigma_{nm+1}U^\sigma_R D^\sigma_R R^\sigma_R\\&=A^\sigma+L^\sigma_L D^\sigma_L W^\sigma_L\Delta^\sigma(i,l)W^\sigma_R D^\sigma_R R^\sigma_R\ .\end{aligned} \tag{25}$$

$\Delta^\sigma(i,l)$ is again given by Eq. (12). The determinant ratio needed to make the decision on flipping the spin is

$$\begin{aligned}R^\sigma&=\frac{\det A^{\sigma'}}{\det A^\sigma}=\det[I+\{W^\sigma_L W^\sigma_R\}^{-1}W^\sigma_L\Delta^\sigma(i,l)W^\sigma_R]\\&=1+[W^\sigma_R\{W^\sigma_L W^\sigma_R\}^{-1}W^\sigma_L]_{ii}\Delta^\sigma(i,l)_{ii}\ .\end{aligned} \tag{26}$$

Notice that R^σ is independent of the matrices $D^\sigma_{L,R}$, R^σ_R, and L^σ_L. In addition, note that the last line of Eq.(26) cannot be simplified further because the $W^\sigma_{R,L}$ are not square matrices.

With the use of Eq. (26) the updating steps can be performed trivially if one knows $\{W^\sigma_L W^\sigma_R\}^{-1}$, which plays a role analogous to that of the equal-time Green's function in the simulation of the grand-canonical ensemble. If $s_{i,l}$ is flipped, then W^σ_L remains unchanged and

$$W_R^\sigma \rightarrow [I+\Delta^\sigma(i,l)]W_R^\sigma = W_R^{\sigma'} . \tag{27}$$

We then see that

$$\{W_L^\sigma W_R^{\sigma'}\}^{-1} = \{W_L^\sigma W_R^\sigma\}^{-1} - \{W_L^\sigma W_R^\sigma\}^{-1} W_L^\sigma \Delta^\sigma(i,l) W_R^\sigma \{W_L^\sigma W_R^{\sigma'}\}^{-1} . \tag{28}$$

The updating of $\{W_L^\sigma W_R^\sigma\}$ can therefore be carried out in $(N^\sigma)^2$ steps. In moving from the l to the $l+1$ times slice, $W_R^\sigma \rightarrow B_{l+1}^\sigma W_R^\sigma$ and $W_L^\sigma \rightarrow W_L^\sigma B_{l+1}^{\sigma -1}$, while $W_L^\sigma W_R^\sigma$ and its inverse remain unchanged.

Suppose we begin on the first time slice and update spins in the direction of increasing l. After updating the first m slices we must make a *UDR* decomposition of $B_m^\sigma, \ldots, B_1^\sigma$. After updating the next m time slices we make a *UDR* decomposition of $B_{2m}^\sigma, \ldots, B_1^\sigma$, and so forth. We save each of these. After updating all time slices we work back in the direction of decreasing l. As we do so, we make *LDU* decompositions of $B_L^\sigma, \ldots, B_{L-m+1}^\sigma$, etc., and store these also. At any one time we need to store a total of L/m decomposed matrices. However, we need only make one decomposition for each block of m time slices that we update. As a result, we use of order

$$[(N^+)^3+(N^-)^3](L/m)$$

numerical operations per sweep of the lattice in performing *LDU* or *UDR* decompositions. We also use of order

$$[(N^+)^3+(N^-)^3]L$$

operations in the updating process including the updating of the inverse matrix via Eq. (28). Thus, the operation count for this algorithm truly scales linearly with β.

III. NUMERICAL RESULTS

The one-band Hubbard model represents an excellent testing ground for new Monte Carlo algorithms. Not only are the physical properties of this model of great current interest, but in addition there are a variety of results available for comparison. Here we apply the algorithms described above to the two-dimensional Hubbard model at half-filling, $\langle n \rangle = 1.0$, and at quarter-filling, $\langle n \rangle = 0.5$.

A. Half-filled band

As has been noted in previous studies,[12,13] for some configurations the determinants $\det M^+$ and $\det M^-$ in Eq. (7) can be negative. In the half-filled Hubbard model, however, particle-hole symmetry implies that the *product* $\det M^+ \det M^-$ is never negative.[12] Off half-filling the product is negative for some configurations, and one must use $|\det M^+ \det M^-|$ as the probability distribution for the Monte Carlo simulation. As we show in the next section, this can limit the temperatures that can be reached at some fillings. However, at half-filling with the algorithm described above, computer time appears to be the only limitation to the size of the lattice and the temperature that can be simulated.

At half-filling, in the strong coupling limit, to second order in t/U the Hubbard model is equivalent to an antiferromagnetic Heisenberg model with Hamiltonian

$$H = J \sum_{\langle ij \rangle} (\mathbf{S}_i \cdot \mathbf{S}_j - \tfrac{1}{4}) , \tag{29}$$

where $\langle ij \rangle$ denotes nearest neighbors and $J = 4t^2/U$. Even for moderate U, simulations have shown strong antiferromagnetic correlations. For the Heisenberg model, recent Monte Carlo simulations strongly support the view that there is long-range order in the ground state.[14] Simulations also suggest that the ground state of the Hubbard model with finite U has long-range order.[5,12] Our present results confirm this. For example, staggered spin correlations are clearly visible in Fig. 1(a), which

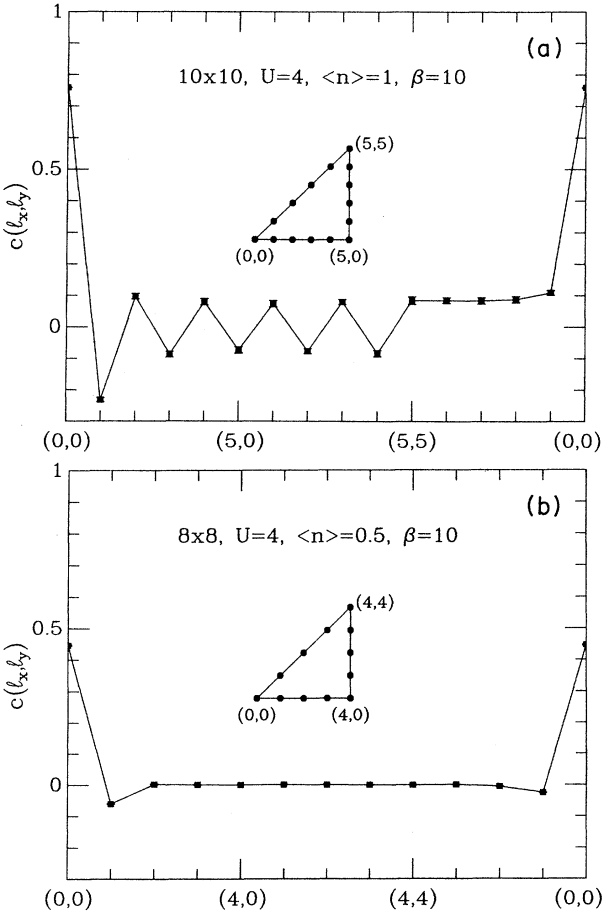

FIG. 1. Spin-spin correlation function $c(l_x,l_y)$. The horizontal axis traces out the triangular path showing in the center of the figure. Strong antiferromagnetic correlations are visible in (a), which is for a half-filled band, but are nearly absent in (b), which is at quarter-filling.

shows the spin-spin correlation function

$$c(l_x,l_y)=\frac{1}{N}\sum_i(-1)^{l_x+l_y}\langle(n_{i+l\uparrow}-n_{i+l\downarrow})(n_{i\uparrow}-n_{i\downarrow})\rangle \tag{30}$$

for a 10×10 lattice with $U=4$, $t=1$, and $\beta=16$. (In all our results $t=1$.) Except where otherwise noted, the calculations were done using the grand-canonical algorithm with $\Delta\tau=0.125$, which resulted in systematic errors of a few percent. At $\beta=16$, the correlation length is clearly much larger than the 10×10 lattice. In contrast, staggered spin-spin correlations are nearly absent in the quarter-filled results shown in Fig. 1(b). The Fourier transform of this correlation functions is the structure factor

$$S(\mathbf{q})=\sum_l e^{i\mathbf{q}\cdot\mathbf{l}}c(l_x,l_y)\ , \tag{31}$$

which is plotted in Fig. 2 for $\langle n\rangle=1.0$ with $q_x=q_y$. For a half-filled band, $S(\mathbf{q})$ peaks at $\mathbf{q}=(\pi,\pi)$, and $S(\pi,\pi)$ is plotted in Fig. 3 versus β for various sized lattices. The zero-temperature canonical ensemble results are shown as the symbols at $\beta=22$. From the figure we see that for the lattice sizes shown, by the time the inverse temperature β is 10 to 15, the system has very nearly reached the ground state. In the zero-temperature algorithm the effective temperature $\gamma+\gamma'$ in Eq. (21) needed for the system to be in the ground state depends on the trial state $|\psi_0\rangle$ used, but is typically ~30. The value of β roughly twice that of the grand-canonical method because the expectation value of the operator O in Eq. (21) is evaluated in the state $e^{-\gamma H}|\psi0\rangle$, and projects out the ground state with an effective temperature γ. The strengths of the zero-temperature method appear to lie in doing low-density calculations and in problems where it is necessary to precisely set the number of particles. In practice, over the range of temperatures and band fillings we have studied, it is faster to obtain zero-temperature results by using the grand-canonical method at low temperature than the zero-temperature method. For the rest of the results present here the grand-canonical method was used.

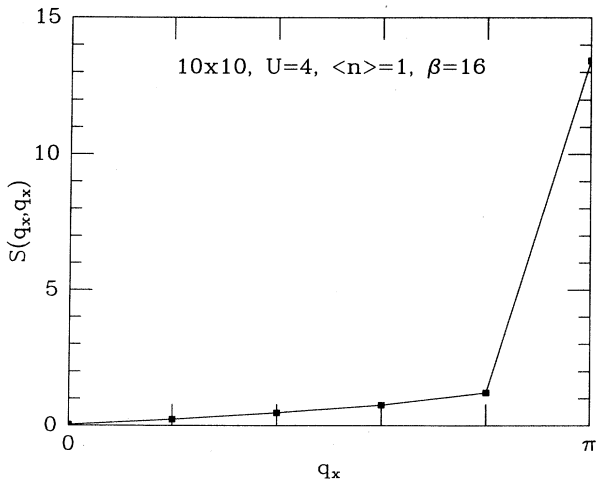

FIG. 2. The magnetic correlation function $S(\mathbf{q})$ for $q_x=q_y$ at half-filling. The function is sharply peaked at $q=(\pi,\pi)$.

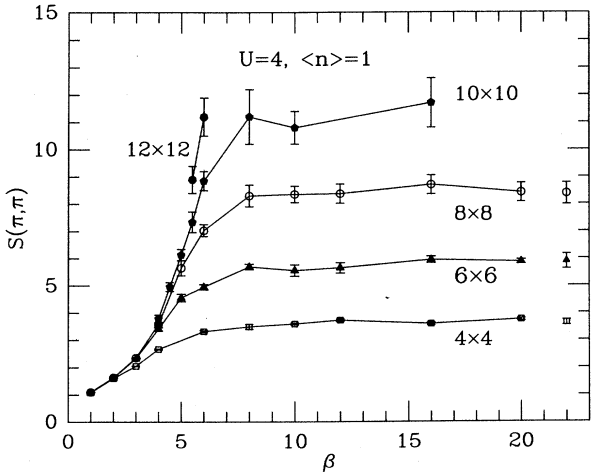

FIG. 3. The antiferromagnetic structure factor $S(\pi,\pi)$ as a function of inverse temperature for a variety of lattice sizes. The points at $\beta=22$ were done with the zero-temperature, fixed particle number algorithm, while the rest were obtained with the grand-canonical algorithm.

From Fig. 3 it is clear that the zero-temperature extrapolation of $S(\pi,\pi)$ increases with lattice size. Within spin-wave theory,

$$\frac{S(\pi,\pi)}{N}=\frac{m^2}{3}+O\left[\frac{1}{\sqrt{N}}\right]\ , \tag{32}$$

with m the antiferromagnetic order parameter. This order parameter can also be obtained by extrapolating to infinite lattice size the zero-temperature limit of the spin-spin correlation function between the two most distant points on a lattice $c(N_x/2,N_x/2)$. Again, according to spin-wave theory,

$$c(N_x/2,N_x/2)=\frac{m^2}{3}+O\left[\frac{1}{\sqrt{N}}\right]\ , \tag{33}$$

with $N=N_x^2$. Using these forms, Eqs. (32) and (33), results for $S(\pi,\pi)/N$ and $c(N_x/2,N_x/2)$ are plotted versus $N^{-1/2}=N_x^{-1}$ in Fig. 4. The values of m^2 which are obtained agree with each other (within statistical errors) as well as with the results reported in Ref. 13.

In Fig. 5 we show the total energy per site as a function of β for lattices ranging in size from 4×4 to 12×12. These lattices are of sufficient size to allow us to obtain the ground-state energy of the infinite system by extrapolation. The statistical errors for the energy are sufficiently small that systematic errors associated with finite $\Delta\tau$ become important. For that reason, we repeated some of the calculations shown in Fig. 5 for $\Delta\tau=0.167$ and 0.083. To a very good approximation, the error in the energy behaved as $\Delta\tau^2$, as expected. Furthermore,

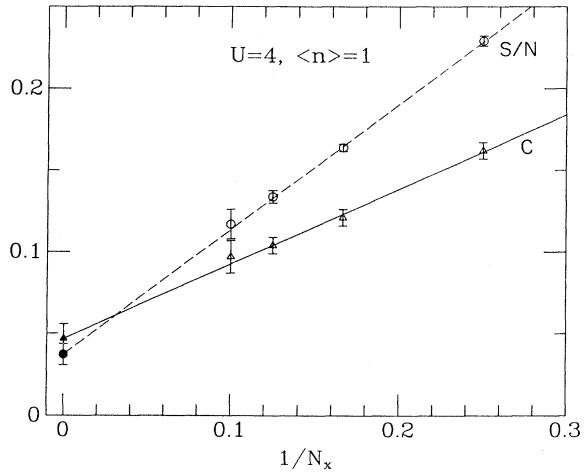

FIG. 4. Plots of $S(\pi,\pi)/N$ (circles) and $c(N_x/2,N_x/2)$ (triangles) vs $1/N_x$. The data was taken from grand-canonical runs at $\beta \geq 16$. The lines are least-squares fits to the data. The extrapolation of these fits to the infinite system are shown as the solid symbols.

the coefficient of the $\Delta\tau^2$ term did not appear to depend on lattice size.[8] From spin-wave theory[15] the finite-size correction to the energy from the infinite-system limit is proportional to N_x^{-3} at $T=0$. By performing a least squares fit to the form

$$E(\Delta\tau,N_x)=E(0,\infty)+a_1\Delta\tau^2+a_2N_x^{-3}\ , \tag{34}$$

we extracted the ground-state energy per site for the infinite system. The extrapolated energy was

$$E(0,\infty)=-0.864\pm0.001\ ,$$

with $a_1=-1.95\pm0.04$ and $a_2=1.59\pm0.13$. Assuming the $\Delta\tau$ errors vary slowly with temperature, using these results to correct for finite $\Delta\tau$ in Fig. 5 would shift the vertical axis by 0.03. The vertical axis on the right is labeled with this correction, and the extrapolated infinite-system result is indicated. A similar fit was performed for the kinetic energy alone. The extrapolated kinetic energy was $E_k(0,\infty)=-1.368\pm0.001$.

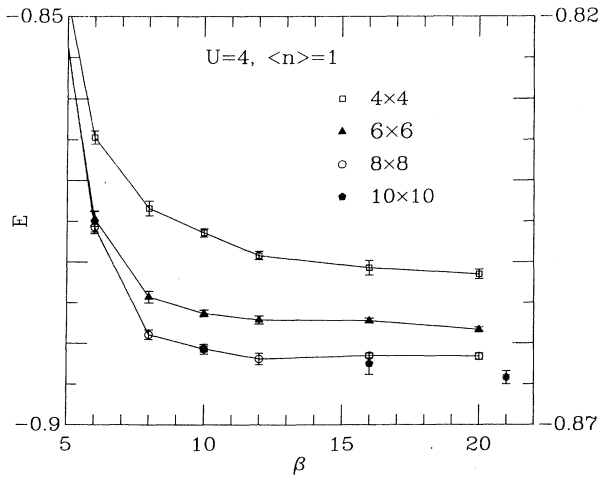

FIG. 5. Total energy $E=E_k+U\langle n^+n^-\rangle$ vs β for a variety of lattice sizes at half-filling. The runs shown have $\Delta\tau=0.125$, and these finite $\Delta\tau$ results correspond to the vertical scale on the left. Correcting the results to $\Delta\tau=0$ gives the scale on the right (see the text). The point at $\beta=21$ is the extrapolation to $T=0$ for an infinite system.

For moderate values of U, the staggered order parameter m is reduced by both the zero point spin fluctuations and charge fluctuations. The charge fluctuations also reduce the size of the local spin moment.[9] The squared local moment $\langle(n_{i+}-n_{i-})^2\rangle$ is plotted versus U in Fig. 6(a), and the related double occupancy $\langle n_{i+}n_{i-}\rangle$ is shown in Fig. 6(b). Clearly, as U increases, a local moment is formed and the double occupancy of a site decreases. At the same time, we expect the effective one-electron transfer to decrease. A measure of this reduction is given by the ratio of the ground-state expectation values of $\langle c_{i\sigma}^\dagger c_{j\sigma}+c_{j\sigma}^\dagger c_{i\sigma}\rangle$ in the presence of the interaction U to its noninteracting value for $U=0$. A plot of this ratio versus U for $\beta=16$ on a 4×4 lattice is shown in Fig. 7. This matrix element can also be obtained from

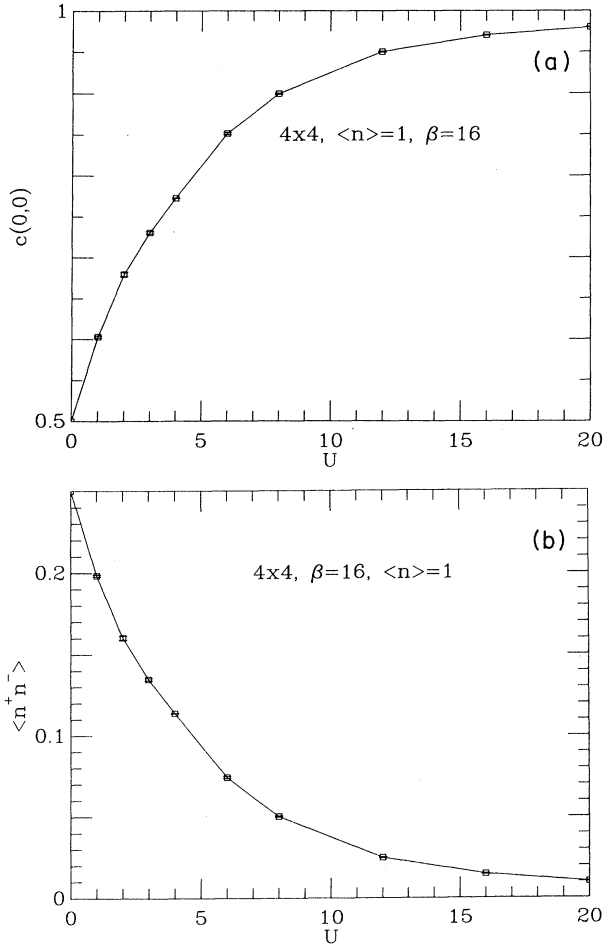

FIG. 6. (a) The squared local moment $c(0,0)=\langle(n_{i+}-n_{i-})^2\rangle$ and (b) the double occupancy $\langle n_{i+}n_{i-}\rangle$ as a function of U. As U increases, a local moment is formed and the double occupancy of a site decreases.

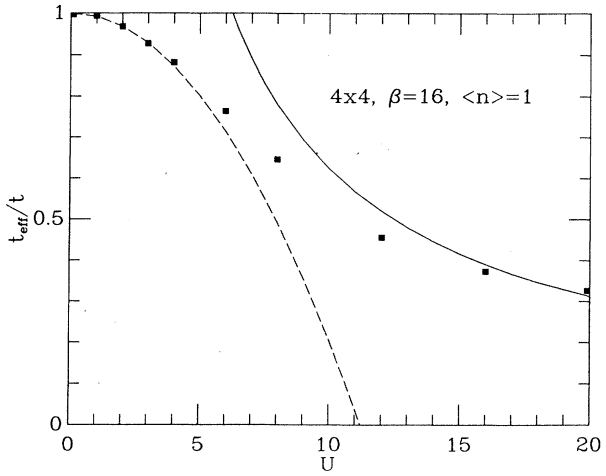

FIG. 7. Reduction in effective hopping as a function of U on a 4×4 lattice for $\beta=16$. The solid line is a strong coupling result. The dashed line is obtained from perturbation theory.

the ground-state energy E_0 by use of the Feynman-Hellman relation

$$\langle c^\dagger_{i\sigma}c_{j\sigma}+c^\dagger_{j\sigma}c_{i\sigma}\rangle=\frac{1}{2N}\frac{\partial E_0}{\partial t}\ . \tag{35}$$

Second-order perturbation theory gives

$$\frac{t_{\rm eff}}{t}=\frac{\langle c^\dagger_{i\sigma}c_{j\sigma}+c^\dagger_{j\sigma}c_{i\sigma}\rangle_U}{\langle c_{i\sigma}c_{j\sigma}+c^\dagger_{j\sigma}c_{i\sigma}\rangle_0}=1-\left[\frac{U}{t}\right]^2\left[\frac{\Delta\varepsilon_2}{\Delta\varepsilon_0}\right]\ , \tag{36}$$

with

$$\Delta\varepsilon_0=\frac{2}{N}\sum_k\varepsilon_k\ , \tag{37}$$

$$\Delta\varepsilon_2=\frac{1}{N^3}\sum_{kk'q}\frac{f(\varepsilon_k)f(\varepsilon_{k'})[1-f(\varepsilon_{k+q})][1-f(\varepsilon_{k'-q})]}{\varepsilon_k+\varepsilon_{k'}-\varepsilon_{k+q}-\varepsilon_{k'-q}}\ .$$

Here,

$$\varepsilon_k=-2t(\cos k_x+\cos k_y)$$

and f is the Fermi factor. This result for $t_{\rm eff}/t$ is shown as the dashed curve in Fig. 7. In the strong coupling limit where (29) applies, the local moment $\langle m_z^2\rangle\to1$ and

$$\frac{t_{\rm eff}}{t}=\frac{4\left[\frac{4t}{U}\right][|\langle\mathbf{S}_i\cdot\mathbf{S}_j\rangle|+\frac{1}{4}]}{|\Delta\varepsilon_0|}\ . \tag{38}$$

Using the value for $|\langle\mathbf{S}_i\cdot\mathbf{S}_j\rangle|=0.335$ obtained for the two-dimensional (2D) Heisenberg model by Reger and Young,[14] one finds the solid line plotted in Fig. 7. These results clearly show that a repulsive Coulomb interaction reduces the one-electron transfer and at the same time gives rise to local moments.

In the half-filled Hubbard model, the particle-hole charge-density fluctuations involve the creation of doubly occupied and empty sites. These excitations involve an energy gap set by U and at zero temperature are expected to lead to an insulating state with a divergent compressibility. The compressibility varies inversely with $\partial\langle n\rangle/\partial\mu$, which within our simulations appears to vanish at half-filling as $T\to0$. A second class of particle-hole excitations involves fluctuations of the spins. In this case, as T goes to zero, we expect these excitations to become the spin waves of the insulating antiferromagnetic state. A useful upper bound for the dispersion relation of these excitations can be obtained from $S(q)$ using a procedure similar to Feynman's treatment of the density fluctuations in ^{4}He.[16]

Consider the trial excited state

$$|\psi_q\rangle=S^z_q|\psi_0\rangle/\langle\psi_0|S^z_{-q}S^z_q|\psi_0\rangle\ , \tag{39}$$

with $|\psi_0\rangle$ the exact ground state and

$$S^z_q=\sum_l e^{iq\cdot l}(n_{l\uparrow}-n_{l\downarrow})\ . \tag{40}$$

Then the excitation energy of this state is

$$\tilde\omega(q)=\langle\psi_q|H|\psi_q\rangle-\langle\psi_0|H|\psi_0\rangle=\frac{2}{3}\frac{E_0}{N}\left[1-\frac{\varepsilon_q}{4}\right]/S(q)\ , \tag{41}$$

with (E_0/N) the ground-state energy per site and $S(q)$ the structure factor, Eq. (31). Figure 8 shows $\tilde\omega(q)$ versus q for a 10×10 lattice with $U=4$. As the size increases, $S(\pi,\pi)$ increases, driving the excitation energy $\tilde\omega(\pi,\pi)$ to zero and generating the expected spin-wave dispersion relation.

We have also calculated the temperature dependence of the $\mathbf{q}=0$ magnetic susceptibility

$$\chi(T)=\left\langle\left[\frac{1}{N}\sum_l(n_{l\uparrow}-n_{l\downarrow})\right]^2\right\rangle\Big/T\ . \tag{42}$$

Figure 9 shows χ versus T for 8×8 lattice with $U=4$. The behavior of $\chi(T)$ is similar to that expected for a two-dimensional Heisenberg antiferromagnet. However, for $U/t=4$, the moment is not fully developed [see Fig. 6(a)] and the itineracy and charge fluctuations still play a role.

B. Non-half-filled band

As discussed above, when the Hubbard model is doped off of half-filling, the finite-temperature simulations become more difficult because of sign problems. In cases where the (unnormalized) probability distribution $P(\{s\})$ is not positive-semidefinite, one uses $|P(\{s\})|$ as the probability distribution, and the expectation value of an observable O is calculated as

$$\langle O\rangle_P=\frac{\langle O\,\mathrm{sgn}P\rangle_{|P|}}{\langle\,\mathrm{sgn}P\rangle_{|P|}}\ , \tag{43}$$

where the subscript P and $|P|$ indicate averages taken in the distributions $P(\{s\})$ and $|P(\{s\})|$, respectively. However, if the average sign, $\langle\,\mathrm{sgn}P\rangle_{|P|}$, is close to zero, this estimator for $\langle O\rangle_P$ is very noisy. Figure 10 shows the average sign versus $\langle n\rangle$ for a various lattice sizes and temperatures. The dramatic fall off of the average sign as

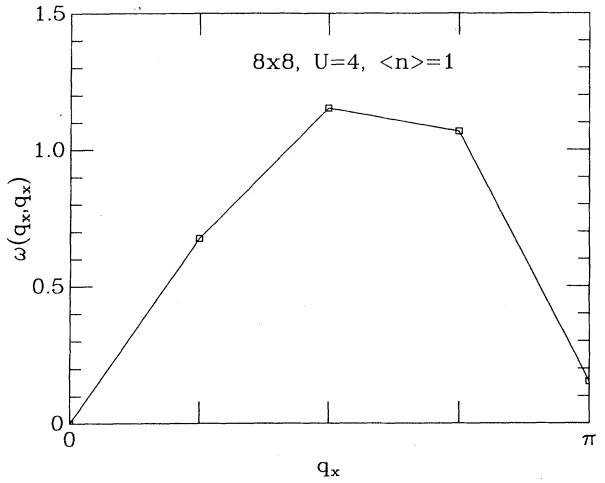

FIG. 8. Spin-wave energy $\omega(q_x,q_x)$ for a 10×10 lattice with $U=4$. This dispersion relation is generated using a procedure similar to Feynman's treatment of the density fluctuations in ^{4}He.

the system is doped away from half-filling makes it difficult to calculate in the interesting filling regime $0.7<\langle n\rangle<0.95$. As shown, in this region the average sign decreases as the spatial and temporal size of the lattice increases. The peak at a filling of 0.625 for the 4×4 lattice is striking. This filling corresponds to the presence of 10 particles, which for the noninteracting system just fills the five lowest k states, leaving a gap to the next empty k state.[17]

Clearly, from Fig. 10 one finds that there is a negligible sign problem for a quarter-filled band, $\langle n\rangle=0.5$. As shown in Fig. 1(b), the staggered spin-spin correlations are nearly absent for $\langle n\rangle=0.5$ and $U=4$. It is also interesting to compare the single-particle momentum occupation $\langle n_{ks}\rangle=\langle c_{ks}^\dagger c_{ks}\rangle$ for half-filling and quarter-filling. Figures 11(a) and 11(b) show $\langle n_{ks}\rangle$ versus $\mathbf{k}=(k,k)$ for an 8×8 lattice with $U=4$ and $\beta=10$ with fillings of $\langle n\rangle=1.0$ and 0.5, respectively. The dashed lines represent the noninteracting Fermi distributions at $\beta=10$. Qualitatively, the distribution for $\langle n\rangle=1.0$ is broadened more by the interaction than for $\langle n\rangle=0.5$

We have also studied the equal time d-wave pair-field correlation function

$$D_d=\langle\Delta_d\Delta_d^\dagger\rangle\ , \tag{44}$$

with

$$\Delta_d^\dagger=\frac{1}{2\sqrt{N}}\sum_{l,\delta}c_{l\uparrow}^\dagger c_{l+\delta\downarrow}^\dagger(-1)^\delta\ . \tag{45}$$

Here, δ sums over the four near neighbor sites of l and $(-1)^\delta$ gives the $+\ -\ +\ -$ sign alternation characteristic of a d-wave pairing amplitude. White *et al.*[18] found that by comparing susceptibilities with uncorrelated susceptibilities (susceptibilities with the interaction vertex moved), one can determine whether the effective pairing interaction is attractive or repulsive. The full and uncorrelated susceptibilities exhibit the same dressed single-quasiparticle effects: differences between them are due to the two-particle effective interaction. White *et al.* found that near half-filling the d-wave susceptibility was

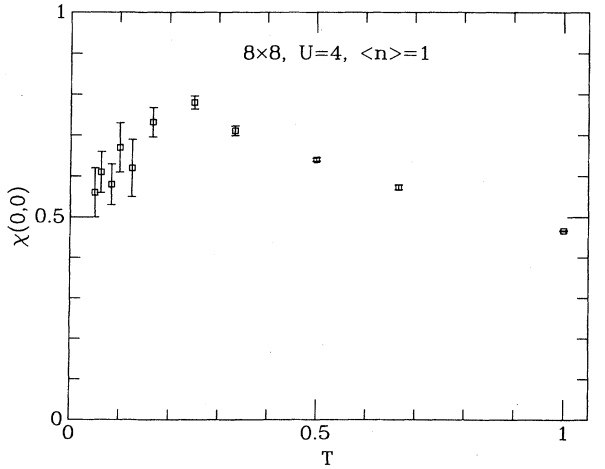

FIG. 9. The $\mathbf{q}=0$ magnetic susceptibility, χ, as a function of T on an 8×8 lattice with $U=4$.

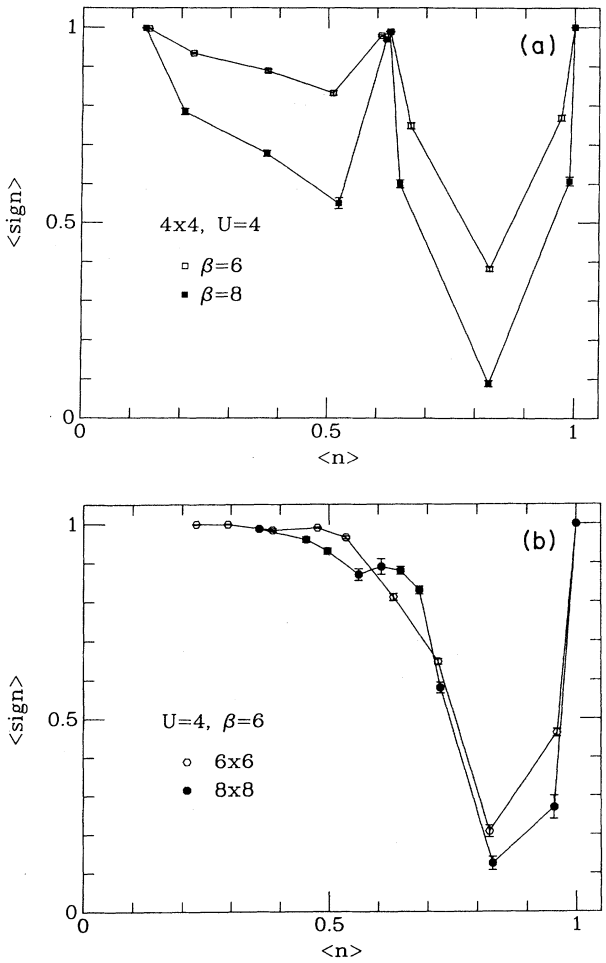

FIG. 10. (a) and (b) Average sign as a function of band-filling for various lattice sizes and temperatures.

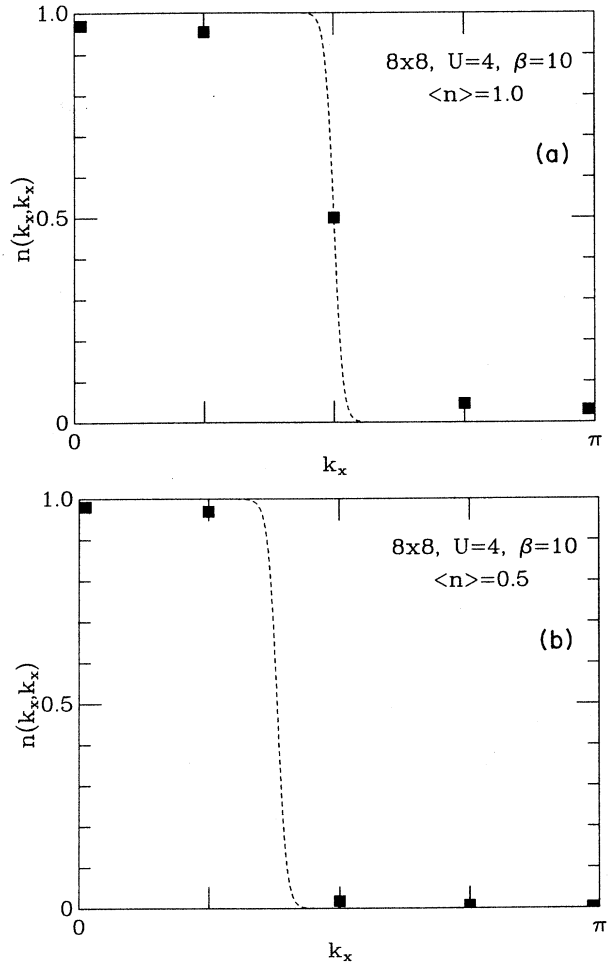

FIG. 11. The momentum distribution $n(\mathbf{k})$ for an 8×8 lattice with $U=4$ and $\beta=10$ at (a) half-filling ($\langle n\rangle=1.0$) and (b) quarter-filling ($\langle n\rangle=0.5$). The dashed curves are the $U=0$ results.

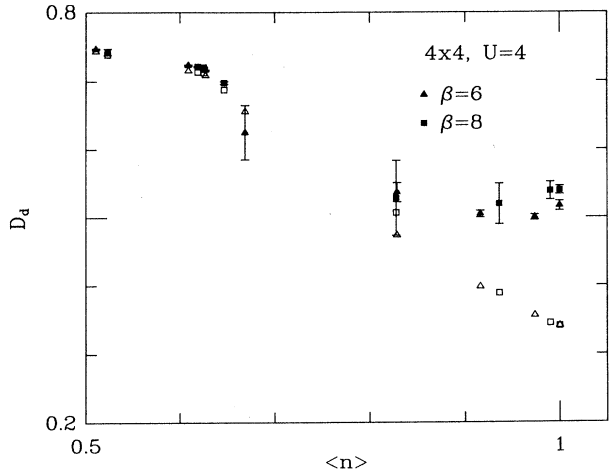

FIG. 12. d-wave pair correlation functions as a function of band-filling. The solid symbols show the full correlation functions, while the open symbols show the corresponding uncorrelated form for which the interaction vertex is removed.

significantly enhanced. One can also compare the pair-correlation functions D with their uncorrelated counterparts $\bar{D}$. The uncorrelated pair-correlation functions corresponding to D_d is

$$\bar{D}_d=\frac{1}{4N}\sum_{\delta,\delta'}\sum_{l,l'}(-1)^{\delta+\delta'}G(l'+\delta',l+\delta)G(l',l)\ , \qquad (46)$$

where $G(l',l)\equiv\langle c_{l'\sigma}c^{\dagger}_{l\sigma}\rangle$. In Fig. 12 we show both D and $\bar{D}$ versus $\langle n\rangle$ for a 4×4 lattice. As in the case of the d-wave pair-field susceptibility, D_d is enhanced over $\bar{D}$ near half-filling. Unfortunately, the fillings where there is enhancement correspond to the region where the sign problem is worst for the simulation, so that very low temperatures cannot be reached (except exactly at half-filling). Hence, the question of whether the attractive interaction ever leads to superconductivity remains open.

IV. SUMMARY

In this paper we have introduced two algorithms which use matrix-decomposition methods to remove the numerical instabilities which have plagued simulations of many-electron systems at very low temperatures, and we have used these algorithms to study the properties of the two-dimensional Hubbard model. The first algorithm gives grand-canonical, finite-temperature results. The second gives ground-state results for a fixed number of electrons. Both algorithms can give ground-state results at half-filling. The grand-canonical algorithm is useful at all fillings, although sign problems, the biggest remaining obstacle to simulations of many-electron systems, can limit the temperatures which can be reached at some fillings. Away from half-filling the ground-state algorithm appears to have more limited usefulness, since sign problems may become overwhelming before the ground state is reached. The main benefit of the ground-state algorithm may lie in problems where the number of particles must be set precisely, such as in determining energy gaps. In addition, at very low fillings the ground-state algorithm may be faster than the grand canonical, because the dimension of the fermion matrix used is the number of particles rather than the number of sites.

Our numerical results on the single-band Hubbard model support previous conclusions concerning magnetic properties. In particular, our results support the existence of long-range order in the ground state at half-filling and the absence of long-range order at quarter-filling. The magnetic susceptibility for a half-filled band with $U/t=4$ shows a temperature dependence similar to that of a two-dimensional antiferromagnet. We have determined the ground-state energy, and obtained an upper bound to the spin wave excitation spectrum. At one-quarter filling, the system appears to be nonmagnetic. Near half-filling, fluctuations in the sign of the fermion determinant make it difficult to perform simulations on large lattices at low temperatures. We have given some results showing how the average sign of the determinant varies with filling, temperature, and lattice size. The behavior of the d-wave pair-field correlation function is

consistent with an attractive d-wave pairing interaction near half-filling.

ACKNOWLEDGMENTS

We would like to thank A. Moreo for discussions and for providing most of the data on the 10×10 and 12×12 lattices shown in Fig. 3. This work was supported in part by National Science Foundation Grants Nos. PHY86-14185, DMR 86-15454, and DMR 86-12860, by Department of Energy Grant No. DE-FG03-88ER45197, and by the San Diego Supercomputer Center. S.R.W. gratefully acknowledges the support of IBM.

[1]An initial report on this work was given by E. Y. Loh, J. E. Gubernatis, R. T. Scalettar, S. R. White, and R. L. Sugar, in *Workshop on Interacting Electrons in Reduced Dimension,* edited by D. Baeriswyl and D. K. Campbell (Plenum, New York, in press).

[2]S. R. White, R. L. Sugar, and R. T. Scalettar, Phys. Rev. B **38**, 11695 (1988); J. E. Hirsch, *ibid.* **38**, 12 023 (1988).

[3]G. Sugiyama and S. E. Koonin, Ann. Phys. **168**, 1 (1986).

[4]S. Sorella, S. Baroni, R. Car, and M. Parrinello, Europhys. Lett. **8**, 663 (1989); S. Sorella, E. Tosatti, S. Baroni, R. Car, and M. Parrinello Int. J. Mod. Phys. B **1**, 993 (1989).

[5]J. E. Hirsch and S. Tang (unpublished).

[6]R. Blankenbecler, D. J. Scalapino, and R. L. Sugar, Phys. Rev. D **24**, 2278 (1981).

[7]M. Suzuki, Prog. Theor. Phys. **56**, 1454 (1976).

[8]R. M. Fye, Phys. Rev. B **33**, 6271 (1986); R. M. Fye and R. T. Scalettar, *ibid.* **36**, 3833 (1987).

[9]J. E. Hirsch, Phys. Rev. B **31**, 4403 (1985).

[10]We use the Trotter approximation to write $\exp(-\Delta\tau K)$ as a product of four sparse matrices. In the "checkerboard" breakup we use, one of these matrices allows hopping between sites (i_x,i_y) and sites (i_x+1,i_y) with i_x even, a second with i_x odd. The third and fourth matrices allow for hopping between sites (i_x,i_y) and (i_x,i_y+1) with i_y even and odd.

[11]A detailed discussion of the use of matrix factorization methods to compute fermion Green's functons for both the grand-canonical ensemble and zero-temperature problems is planned to be given by E. Y. Loh, J. E. Gubernatis, R. T. Scalettar, S. R. White, and R. L. Sugar (unpublished).

[12]J. E. Hirsch, Phys. Rev. B **31**, 4403 (1985).

[13]S. R. White and J. W. Wilkins, Phys. Rev. B **37**, 5024 (1988).

[14]J. D. Reger and A. P. Young, Phys. Rev. B **37**, 5978 (1988).

[15]D. A. Huse, Phys. Rev. B **37**, 2380 (1988).

[16]R. P. Feynman, Phys. Rev. **94**, 262 (1954).

[17]S. Sorella has suggested that the sign problems appear to be reduced at fillings corresponding to nondegenerate ground states of the noninteracting systems (private communication).

[18]S. R. White, D. J. Scalapino, R. L. Sugar, N. E. Bickers, and R. T. Scalettar, Phys. Rev. B **39**, 839 (1989).